

Similar local neuronal dynamics may lead to different collective behavior

Margarita M. Sánchez Diaz^{1,2}, Eyisto J. Aguilar Trejo^{1,2,3}, Daniel A. Martín^{1,2,3}, Sergio A. Cannas,^{3,4} Tomás S. Grigera^{1,3,5,6} and Dante R. Chialvo^{1,2,3}

¹Center for Complex Systems and Brain Sciences (CEMSC), Universidad Nacional de San Martín, Campus Miguelete, 25 de Mayo y Francia, 1650 San Martín, Buenos Aires, Argentina

²Instituto de Ciencias Físicas (ICIFI), CONICET and Universidad Nacional de San Martín, 25 de Mayo y Francia, 1650 San Martín, Buenos Aires, Argentina

³Consejo Nacional de Investigaciones Científicas y Técnicas (CONICET), Godoy Cruz 2290, 1425 Buenos Aires, Argentina

⁴Instituto de Física Enrique Gaviola (IFEG-CONICET), Facultad de Matemática Astronomía Física y Computación, Universidad Nacional de Córdoba, 5000 Córdoba, Argentina

⁵Instituto de Física de Líquidos y Sistemas Biológicos (IFLySiB), CONICET and Universidad Nacional de La Plata, Calle 59 no. 789, B1900BTE La Plata, Buenos Aires, Argentina

⁶Departamento de Física, Facultad de Ciencias Exactas, Universidad Nacional de La Plata, 1900 La Plata, Buenos Aires, Argentina



(Received 24 July 2021; revised 5 November 2021; accepted 10 December 2021; published 29 December 2021)

This report is concerned with the relevance of the microscopic rules that implement individual neuronal activation, in determining the collective dynamics, under variations of the network topology. To fix ideas we study the dynamics of two cellular automaton models, commonly used, rather in-distinctively, as the building blocks of large-scale neuronal networks. One model, due to Greenberg and Hastings (GH), can be described by evolution equations mimicking an integrate-and-fire process, while the other model, due to Kinouchi and Copelli (KC), represents an abstract branching process, where a single active neuron activates a given number of postsynaptic neurons according to a prescribed “activity” branching ratio. Despite the apparent similarity between the local neuronal dynamics of the two models, it is shown that they exhibit very different collective dynamics as a function of the network topology. The GH model shows qualitatively different dynamical regimes as the network topology is varied, including transients to a ground (inactive) state, continuous and discontinuous dynamical phase transitions. In contrast, the KC model only exhibits a continuous phase transition, independently of the network topology. These results highlight the importance of paying attention to the microscopic rules chosen to model the interneuronal interactions in large-scale numerical simulations, in particular when the network topology is far from a mean-field description. One such case is the extensive work being done in the context of the Human Connectome, where a wide variety of types of models are being used to understand the brain collective dynamics.

DOI: [10.1103/PhysRevE.104.064309](https://doi.org/10.1103/PhysRevE.104.064309)

I. INTRODUCTION

The animal brain is composed of billions of neurons, which interact with each other through thousands of synapses per neuron. The results of such interaction is the emergence of complex spatiotemporal patterns of neuronal activity supporting perception, action and behavior. A recent proposal considers the brain as a network of neurons poised near a dynamical transition [1–4], a view which is supported by experimental results gathered from animals both *in vitro* [5] and *in vivo* [6] as well as from whole brain neuroimaging human experiments [7–9].

The potential existence of critical phenomena in the brain motivated, during the last decade, the study of mathematical models to explore better the large-scale brain dynamics. A distinctive difference between the diversity of models is at the microscopic level. Some models consist of networks of simplified neurons, in which neurons themselves are represented by a wide variety of approaches, ranging from two-state

particles [10] through discrete cellular automata [11–14], branching processes [6,15–18], neural masses [19], coupled-maps [20–23], and coupled Kuramoto oscillators [24] up to detailed equations describing the evolution and spiking of the membrane potential [25–27]. Thus, a natural question arises on how relevant the microscopic process (used to represent the individual neuronal dynamics) may be, and how they affect the dynamical collective repertoire exhibited by the network.

When focusing on collective properties, it is of course reasonable to seek minimal models which, even orphan of realistic microscopic rules, may reproduce relevant macroscopic behavior. However, it is not straightforward to determine in principle how general this assumption can be in the case of neuronal networks. Our point is that even though the use of realistic microscopic dynamics is not necessarily a prerequisite to correctly describe universal macroscopic properties, *microscopic rules do matter* and eventually can lead to different universal behavior. As a clarifying metaphor, consider the Ising model. It is well known that algorithms with unre-

alistic nonlocal moves (so-called cluster algorithms [28]) can correctly describe the static critical behavior. However, if the dynamic rule did not follow detailed balance, then the modified dynamics would fail to reproduce equilibrium behavior, even if it could reproduce some sort of critical dynamics. And of course, even with detailed balance, the dynamical universality is altered by the nonlocal rule. A similar correspondence among microscopic rules and system's dynamics appears when modeling brain dynamics, which is rarely considered, thus some extrapolations to real brain dynamics taken from numerical simulations in the current literature, may be hampered by the limitations of the microscopic details of the neuronal models employed. We are purposely not considering here a large chapter of models that include synaptic plasticity.

In this article, we illustrate the problem by studying the dynamics of two apparently similar neural network models: that of Greenberg and Hastings [29] as described in Refs. [11,12] and that of Kinouchi and Copelli [15]. The main difference between these two models is related to the microscopic rule that propagates the activity: the first proposes (as many others of the same kind) a neuronal interaction rule that depends on the state of its presynaptic neighbors, while the second introduces a rule that, regardless of the number of connections, maintains a prescribed branching of activity on the target neurons. At first sight the differences seem innocent-looking, but as it will be shown, they lead to completely different behavior of the network: the first model exhibits continuous or discontinuous phase transitions depending on the network topology, while the second is completely insensitive to it.

We remark from the outset that the article's aim is not to criticize any given model in particular, but to call the attention on the consequences of using them ignoring the limitations of the model's original formulation, including possible misinterpretations. The article is organized as follows: in Sec. II we describe both models and the observables that will be used to characterize the dynamical regimes, in Sec. III we show the results of the numerical simulations, and in Sec. IV we discuss present results in the context of recent research and we summarize the conclusions.

II. NETWORK, MODELS, AND OBSERVABLES

A. The interaction network

Both neuronal models are studied on an undirected Watts-Strogatz small-world network [30] with average connectivity $\langle k \rangle$ and rewiring probability π . The network is constructed as usual [30] by starting from a ring of N nodes (always $N = 20\,000$ in this report), each connected symmetrically to its $\langle k \rangle/2$ nearest neighbors; then each link connecting a node to a clockwise neighbor is rewired to a random node with probability π , so that average connectivity is preserved. The rewiring probability is a measure of the disorder in the network: for $\pi = 0$ the network is circular and perfectly ordered, while for $\pi = 1$ it becomes completely random.

In both models neurons are represented as nodes on a weighted undirected random graph with an associated discrete state variable, $S_i = 0, \dots, n$, where $i = 1, \dots, N$ identifies the node and $S_i = \{0, \dots, n\}$. State 0 represents a quiescent (but excitable) neuron, 1 is the active state, and $2 \dots n$ are

refractory states. The links of the graphs are represented by the $N \times N$ connectivity matrix W . Nonzero matrix elements indicate the presence of a link with a given weight. Weights are positive reals, so $W_{ji} \geq 0$, and the connectivity matrix is symmetric, $W_{ij} = W_{ji}$, since the graph is undirected. In this context, symmetric connections need to be interpreted as two connections between any pair of nodes. Neither the connectivity nor the weights depend on time (i.e., we consider quenched disorder). The dynamical evolution is given by a discrete-time Markov process in which all sites are simultaneously updated, and with transition probabilities for each site given by the expressions below for each model.

1. GH model

This model was introduced by Greenberg and Hastings [29] to mimic the excitable dynamics generically observed in neurons, forest fires, cardiac cells, chemical reactions and epidemic propagation. In the context of brain dynamics it was used recently by Haimovici *et al.* [11]. Here we follow closely the implementation of Zarepour *et al.* [12]. It is a cellular automaton endowed of the three states common to excitable dynamics: quiescent, active, and refractory state, and the dynamics of site i is updated by

$$P_{i,0 \rightarrow 1} = 1 - [1 - r_1] \left[1 - \Theta \left(\sum_{j=1}^{k_{in,i}} W_{ji} \delta_{S_j,1} - T \right) \right], \quad (1a)$$

$$P_{i,1 \rightarrow 2} = 1, \quad (1b)$$

$$P_{i,2 \rightarrow 0} = r_2, \quad (1c)$$

where $P_{i,a \rightarrow b}$ is the probability that site i will transition from state a to state b , at time $t + 1$, S_i is computed at time t , and the sum is performed over all j targeting i and $k_{in,i}$ is the in-degree of node i . $\Theta(x)$ is Heaviside's step function [$\Theta(x) = 1$ for $x \geq 0$ or 0 otherwise], $\delta_{i,j}$ is Kronecker's δ , and r_1 , r_2 , and T are control parameters which are set equal to all sites in the present work. Thus, an active site always turns refractory in the next time step, and a refractory site becomes quiescent with probability r_2 . The probability for a quiescent site to become active is written as 1 minus the product of the probabilities of *not* becoming active through the different mechanisms at work. In this model there are only two activation mechanisms: *spontaneous activation*, which occurs with a small probability r_1 , or *transmitted activation*, which occurs deterministically¹: neuron i will become active if and only if it is in the quiescent state and the sum of the weights of the links connecting i to its active neighbors exceeds a threshold T [see Fig. 1(a)]. The nonnull weights are drawn from an exponential distribution, $p(W_{ji} = w) = \lambda e^{-\lambda w}$, with $\lambda = 12.5$ chosen to mimic the weight distribution of the human connectome [12]. For the simulations described here, we use $r_1 = 0.001$, $r_2 = 0.3$ as in previous work [11,12] which remain fixed in all simulations, while T is used as control parameter.

¹Although the transmitted activation rule is clearly deterministic, we have decided to write it as a transition probability, to make a similar description for both models. This is achieved using a Heaviside function in Eq. (1a).

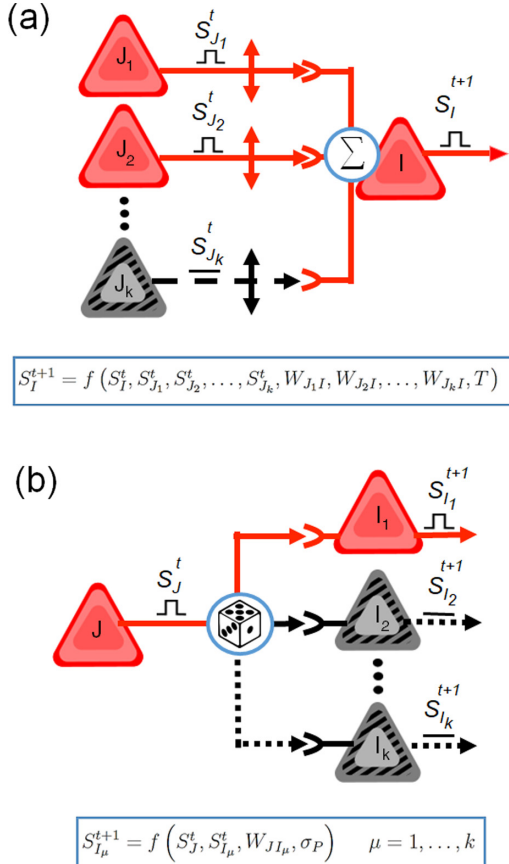


FIG. 1. Rule for the propagation of activity in both models. (a) In the GH model, a given neuron I will become active at time $t + 1$, if the contribution of all active presynaptic neurons (here J_1 and J_2), weighted by the interaction W_{JI} surpasses the threshold T . At each time step, this update is repeated for all quiescent neurons I . (b) In the KC model a given active neuron J will activate at time step $t + 1$ a given number of I neurons depending on the W_{JI} and σ_p value. Note that σ_p normalizes such probability by the number of interactions $\langle k \rangle$. At each time step, this update is repeated for all active neurons J . In both panels, triangles represent neurons and lines synaptic interactions. Red filled triangles denote active neurons and gray dashed ones inactive neurons, at times t and $t + 1$. A summation term in panel (a) indicates that the outcome of neuron I depends on the sum of the contribution of neurons J_1 to J_n , while a dice in panel (b) indicates that stimulated neurons are randomly chosen by J .

2. KC model

This model was introduced by Kinouchi and Copelli [15] to show that a (Erdős–Renyi undirected) network of excitable elements has its sensitivity and dynamic range maximized at the critical point of a nonequilibrium phase transition. The model resembles a branching process [31,32] in which the transition probabilities for neuron i at time $t + 1$ are

$$P_{i,0 \rightarrow 1} = 1 - [1 - r_1] \prod_{j=1}^{k_{in,i}} [1 - pW_{ji}\delta_{S_j,1}], \quad (2a)$$

$$P_{i,1 \rightarrow 2} = 1, \quad (2b)$$

$$P_{i,2 \rightarrow 3} = 1, \quad (2c)$$

$$\vdots \quad (2d)$$

$$P_{i,n \rightarrow 0} = 1.$$

S_j is evaluated at t , and the product is taken over all neurons j pointing to i . The interaction matrix is symmetric, $W_{ij} = W_{ji}$, and nonnull elements are taken uniformly from $[0,1]$. The interaction rule in Eq. (2a) contains two parameters: r_1 which (as in the GH model) determines the spontaneous activity of any inactive neuron and p which controls the transmitted activation probability [see Fig. 1(b)]. This rule makes the main difference with the GH model. If the variance of the chosen values for k_{out} and W are relatively small (as in Ref. [15]), and $\langle k \rangle$ is relatively large, each active neuron will excite, on average $\sigma_p := (\langle k \rangle - 1)p/2$ neurons. Thus, σ_p is an approximate of the desired branching ratio. Similar to the GH model, an active site always becomes refractory, but instead of recovering randomly, here it becomes quiescent deterministically after $n - 1$ time steps. We note that this difference has no relevance for the present analysis.

It is known that, for a wide variety of conditions, critical dynamics is expected for $\sigma_p \simeq 1$ [31]. The critical value of σ_p will be exactly 1 only in the limit of very large networks ($N \rightarrow \infty$), with homogeneous degree distribution, without triangles (i.e., a clustering coefficient equal to zero), and where the dynamics is in the limit of negligible spontaneous activation ($r_1 \rightarrow 0$). For finite values of r_1 , several unrelated activity (i.e., avalanches) may coexist. Under this situation, the system may belong to a different universality class [33]. For a comprehensive analysis on the role of spontaneous activation on modifying the universality class, and how it may also shift the critical value of the branching ratio, we refer the reader to Ref. [33] and references therein. In the following, we will use σ_p instead of p as the control parameter. This choice does not affect the dynamics since both quantities are proportional. Examples of the results as a function of p instead of σ_p can be found in the Supplemental Material [34].

For the simulations, values of $r_1 = 0.001$, and $n = 4$ (i.e., a fixed refractory period of three steps) are chosen, which remain fixed in all simulations. In passing, please notice that the interaction rule in the KC model is entirely stochastic and that neurons behave independently (as long as the spontaneous activity is relatively low as dictated by the value of r_1 used here). Additional details can be found in Costa *et al.* [35] and Campos *et al.* [36]. The numerical implementation of the KC model admits a few variations which, nonetheless, do not change the present results (see the Supplemental Material [34]).

B. Observables

To describe the state of the network, for both models, we define an order parameter $f_S(t)$ which corresponds to the fraction of active neurons at time t ,

$$f_S(t) = \frac{1}{N} \sum_i \delta_{S_i(t), 1}. \quad (3)$$

After any transient dies out, we also compute its variance, $\sigma_{f_S}^2 = \langle f_S^2 \rangle - \langle f_S \rangle^2$, where $\langle \dots \rangle$ is a time average.

For the purposes of the present work, it is of particular interest the behavior of the (normalized) connected

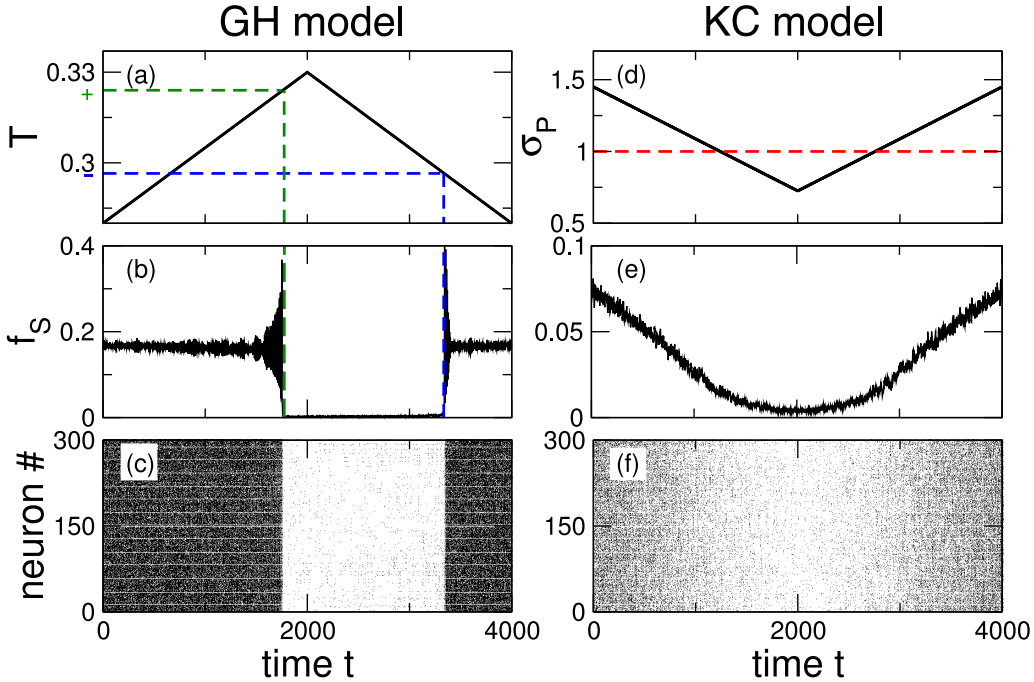


FIG. 2. Examples of the evolution of the activity as the respective control parameter (T or σ_p) is slowly varied. Left panels (a–c) correspond to the GH model and right panels (d–f) to the KC model. Top panels: value of the control parameters [T in panel (a) and σ_p in panel (d)] as a function of time t . Center panels: order parameter $f_S(t)$ for both models as a function of time. Bottom panels: raster plots of 300 selected neurons. Dashed lines in panels (a) and (b) mark the approximate values of T_{\pm} , and their respective times. In both cases $\langle k \rangle = 30$, $\pi = 0.6$. For the GH model, $\Delta T = \pm 0.000025$, and for the KC model $\Delta \sigma = \pm 0.00036$.

autocorrelation of the order parameter f_S ,

$$\rho(\Delta t) = \frac{1}{\sigma_{f_S}^2} \langle (f_S(t) - \langle f_S \rangle) \times (f_S(t + \Delta t) - \langle f_S \rangle) \rangle, \quad (4)$$

which estimates the linear correlation between the network state at times t and $t + \Delta t$, with $\rho(\Delta t) \simeq 1$ for highly correlated consecutive configurations and $\rho(\Delta t) \simeq 0$ when the configurations quickly decorrelate. It is known that the autocorrelation function is sensitive to the different dynamical regimes: close to a continuous phase transition, the dynamics undergoes critical slowing down, which implies that the autocorrelation function decays slower than in the supercritical or subcritical state [37]. For discontinuous phase transitions, a similar effect takes place at the spinodal points [38]. Here we focus on the autocorrelation at $\Delta t = 1$, $\rho(1)$, also called first correlation coefficient, which has been shown to have a maximum at the transition point [37].

C. Parametric exploration

In this work we are interested in exploring the extent of the dynamical repertoire that each model is able to exhibit under a very wide range of: (1) neuronal dynamics and (2) topology of the underlying network. Thus, we proceed to scan the control parameter of the given neuron model for different network topologies (by varying $\langle k \rangle$ and π). This implies to explore three parameters while classifying the dynamical regimes observed.

To identify and classify the dynamical regimes, we track the behavior of $\rho(1)$ as the control parameter (T or σ_p) is increased and decreased. This is repeated for each

combination of network parameters $\langle k \rangle$ and π . The simulations start at T_0 (or σ_0) (using a random initial condition for each neuron) and then it is increased by ΔT (or $\Delta \sigma$) after a given number of steps, up to a final value T_F (or σ_F), without resetting the neuron states when changing the value of the control parameter. This parametric exploration allows us to determine the full repertoire of dynamical regimes which can emerge from the microscopic activity propagation rules acting on a given network topology.

III. RESULTS

A. Characterizing the transitions

Now we proceed to describe how the dynamical repertoire of each model is determined from a parametric exploration. An example is presented in Fig. 2 where panels on the left correspond to results obtained from the GH model and those on the right from the KC model. The figure shows that, as expected, the rate of activity changes as a function of its control parameter, but already demonstrating an important difference between the dynamical regimes exhibited by the two models. For this particular choice of topology, $\langle k \rangle = 30$ and $\pi = 0.6$, the GH model undergoes a discontinuous transition demonstrated by the abrupt change in f_S (also noted in the appearance of the raster plot) and the presence of hysteresis. In contrast, in response to similar parametric scan, the KC model exhibits a continuous transition and does not show hysteresis. In addition, it is important to note that the GH model shows a large increase in the variability of the order parameter f_S near the transition [see Fig. 2(b)], meanwhile the variance of the f_S fluctuations shown by the KC model is relatively constant [see

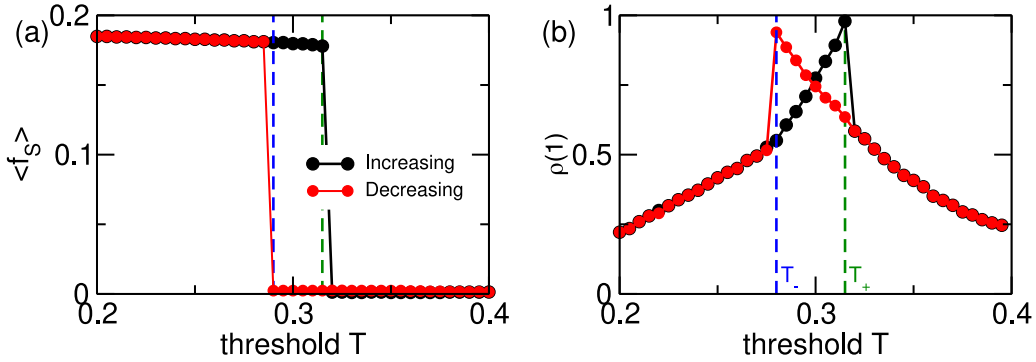


FIG. 3. Evolution of the order parameter $\langle f_S \rangle$ and its autocorrelation $\rho(1)$ as a function of the control parameter T in the GH model. (a) Fraction of active neurons vs threshold T . (b) First autocorrelation coefficient $\rho(1)$ vs threshold T . In both panels the transition points, T_- and T_+ , are marked with vertical dashed lines. Simulations were performed in a network with $\langle k \rangle = 30$ and $\pi = 0.6$. Simulations started at $T_0 = 0$ and neurons in a random state. T was slowly increased by $\Delta T = 0.0025$ every 10^5 time steps up to $T_F = 0.9$, then it was decreased back to T_0 in the same way.

Fig. 2(e)], regardless of the value of the control parameter σ_p . These observations point to important dynamical differences between the two models, as will be expanded in the next sections.

The behavior of the autocorrelation function of the order parameter helps to identify the type of phase transition because it is known to peak near a transition. We compute $\rho(1)$ for each value of the control parameter, and define T_+ as the value that maximizes $\rho(1)$ in a run when T is being increased, and T_- as the value that maximizes $\rho(1)$ when decreasing T . An example for the GH model is presented in Fig. 3. For the KC model, we defined in the same way σ_p+ and σ_p- , although we never observed discontinuous transitions in that model. Results for the KC model for the same conditions and network topologies as in Fig. 3 are shown in the Supplemental Material [34].

Thus, according to the shape of the curves of $\rho(1)$ versus control parameters, we can classify the dynamical behavior: If $\rho(1)$ is monotonic, then there is no phase transition, corresponding to the cases in which the network, after a transient, goes quiescent. For network topologies in which $|T_+ - T_-| \geq 2\Delta T$ (or $|\sigma_+ - \sigma_-| \geq \Delta \sigma_p$) the transition is considered discontinuous and continuous otherwise. In other words, after exploring a reasonable range of values of the control parameter, the existence of a maximum in the $\rho(1)$ curve indicates (under the present context) a phase transition, which is considered continuous if there is no noticeable hysteresis or discontinuous otherwise.

An example of the behavior of $\rho(1)$ in the case of a continuous transition is shown in Fig. 4. This type of transition is observed in both models for a wide range of $\langle k \rangle$ and π values, as will be described in the next section. It can be seen that a change of the control parameter on a range of values near the critical point is reflected on a nonmonotonic change of the $\rho(1)$. The plots in the bottom panels illustrate the typical autocorrelation function of the order parameter f_S . For control parameter values larger than T_c (or smaller than σ_c) the activity correlation vanishes quickly as indicated by the green triangle data points. In the other extreme, for control parameter values smaller than T_c (or larger than σ_c , i.e., data points plotted as blue circles) the function shows an oscillatory pattern. The

first zero crossing of the function is dictated by the duration of the refractory period of the neuronal models which is one of the determinants of the collective oscillation frequency. Finally, for values sufficiently close to T_c (or σ_c) the function $\rho(\Delta t)$ decays very slowly (as a power law) as shown in the figure by the data points plotted with red squares.

B. Models's dynamical repertoire on parameter space

Here we describe the results of a systematic exploration of the collective dynamics as a function of network topology in each model. For each value of $\langle k \rangle$ and π , we computed 5 realizations of Watts-Strogatz graphs. In each case we classified the regimes as a function of the control parameter, according to the behavior of $\rho(1)$ as explained above. The dynamical regimes found include *transients to no-activity*, *continuous phase transition* or *discontinuous phase transition (from no-activity to collective oscillations)*.

The results in Fig. 5 show the regions of parameters at which each regime was observed. In brief, both models exhibit no-transition for network topologies with $\langle k \rangle = 2$ and connectivity disorder $\pi > 0$ (red zone with squares in Fig. 5). For $\pi = 0$ the same regime extends to $\langle k \rangle < 6$ in both models.

For networks with relatively large values of $\langle k \rangle$ both models exhibit a *continuous phase transition* as in the example featured already in Fig. 4 (black zone with circles in Fig. 5). The main difference between the models is found for relatively high values of degree and disorder. At this region of parameters, the GH model shows a discontinuous phase transition (blue zone with triangles), while the KC model presents a continuous one. The inset in Fig. 5(a) shows the border *continuous* and *discontinuous* regions, as a function of network parameters, in a double logarithmic scale. A straight separation line, similar to the one observed by Zarepour *et al.* [12] in the context of cluster size distribution, is observed.

Close to the border between the *continuous transitions* and the *continuous transitions* region, there is a narrow range of $\langle k \rangle$ values for which some realizations of KC model show *continuous transitions*, while other realizations show *discontinuous transitions*. In those cases, the reported kind of transition was determined by the most frequent result. We

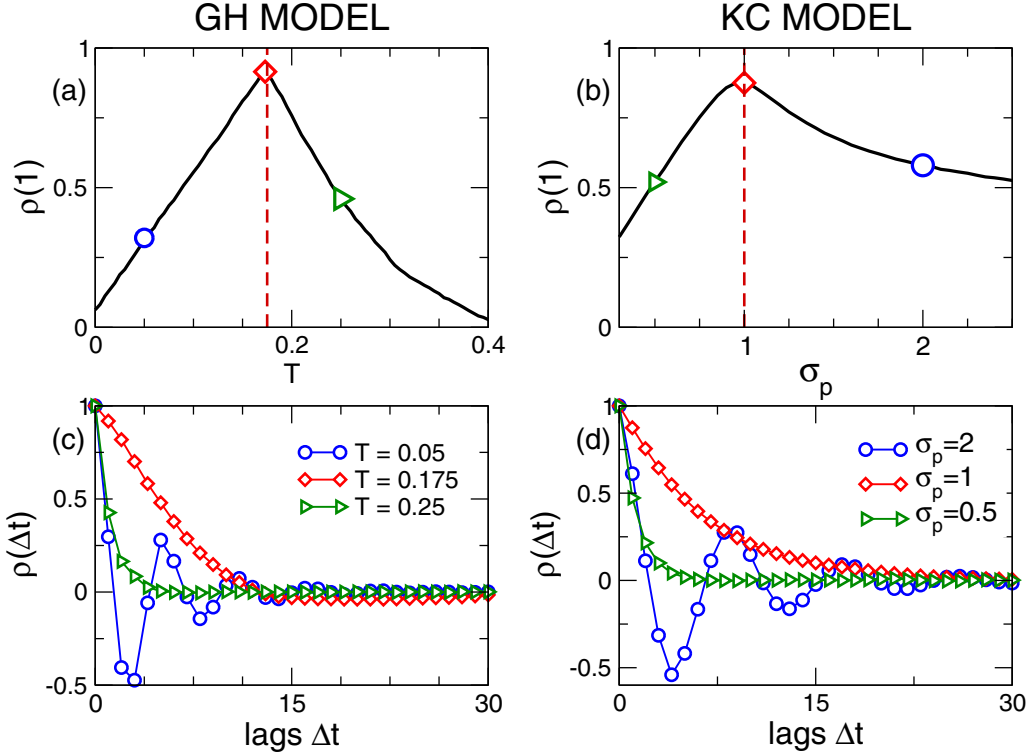


FIG. 4. Behavior of the first autocorrelation coefficient and the autocorrelation function for network parameters resulting in a continuous phase transition. Top panels: first autocorrelation coefficient $\rho(1)$ vs the control parameter, T for the GH model (a) and σ_p for the KC model (b). Bottom panels: Autocorrelation function $\rho(\Delta t)$ vs time lag Δt , for three values of the control parameter, in the supercritical, critical, and subcritical phases, for the GH model (c) and the KC model (d). Dotted lines in panels (a) and (b) denote the critical point and symbols indicate the values of the control parameters used to compute the data in panels (c) and (d). Network parameters: $\langle k \rangle = 10$, $\pi = 0.6$.

have added error bars to Fig. 5(a), whose width is half of the range of $\langle k \rangle$ values for which this coexistence was observed. We did not observe a similar effect at the boundary between *no-activity* to *continuous transition* regions.

The results in Fig. 6 are representative examples of the behavior of $\rho(1)$ as a function of the control parameter for selected values of $\langle k \rangle$ and π . For the GH model, the largest values of $\langle k \rangle$ and π show clear hysteresis, with the peaks for the case of increasing T at a higher value than the peak found when it is decreased. In most cases, the increasing and decreasing sweeps of control parameter yield the same curve, with a maximum value of $\rho(1)$ close to 1. For $\pi = 0$, the (single) peak tends to be rather broad. Finally, for $\langle k \rangle = 2$ and any value of π , and for $k = 4$, $\pi = 0$, $\rho(1)$ behaves monotonically, which is indicative of no phase transition. The KC model shows less variation among the curves, with only a narrow range of monotonous curves, and most of the $\langle k \rangle$, π plane yielding continuous transitions, presenting very similar $\rho(1)$ curves as a function of σ_p .

Finally, the results on Fig. 7 show examples of the spiking patterns observed as the control parameter is increased, for the same selected values of $\langle k \rangle$ and π illustrated in Fig. 6. The patterns were obtained by varying the control parameters from 3% below T_c (or T_+ in the discontinuous case) to 3% above (or from 3% above to 3% below the critical value of σ_p for KC model), and recording the spikes of 300 neurons along 300 time steps. We have used $T = 0$ or $\sigma = 2$ for networks showing no phase transition. For the GH model, there are

several cases (blue raster plots) of discontinuous transitions where there is a sharp decrease of activity after crossing T_+ . Continuous transitions with large $\langle k \rangle$ (such as $\langle k \rangle = 20$, $\pi \geq 0.4$), show bursts of synchronized activity that disappear for T slightly above T_c (black raster plots). Smooth changes in neuron activity are observed for continuous transitions with smaller values of $\langle k \rangle$. Finally, for $\pi = 0$ the network topology corresponds to a circle (or to a torus for larger $\langle k \rangle$ values), so that neurons spiking at time $t + 1$ are close neighbors of those spiking at time t , leading to linear wave-like propagation. Similar to what is observed in the previous figure, KC results show a reduced variety of behavior, where neither discontinuous transitions, nor bursts of synchronized activity are observed close to the critical point.

IV. DISCUSSION

Summarizing, we have revisited two simplified models of neuronal activation to show that subtle differences in the local dynamical rules may result in very different collective dynamics when embedded on networks. We found that the KC model dynamical repertoire includes, as a function of its control parameter, only continuous phase transitions being, by design, insensitive to the network topology. This is at odds with the GH model, in which each neuron outcome is influenced by its connectivity degree and therefore by the overall network topology.

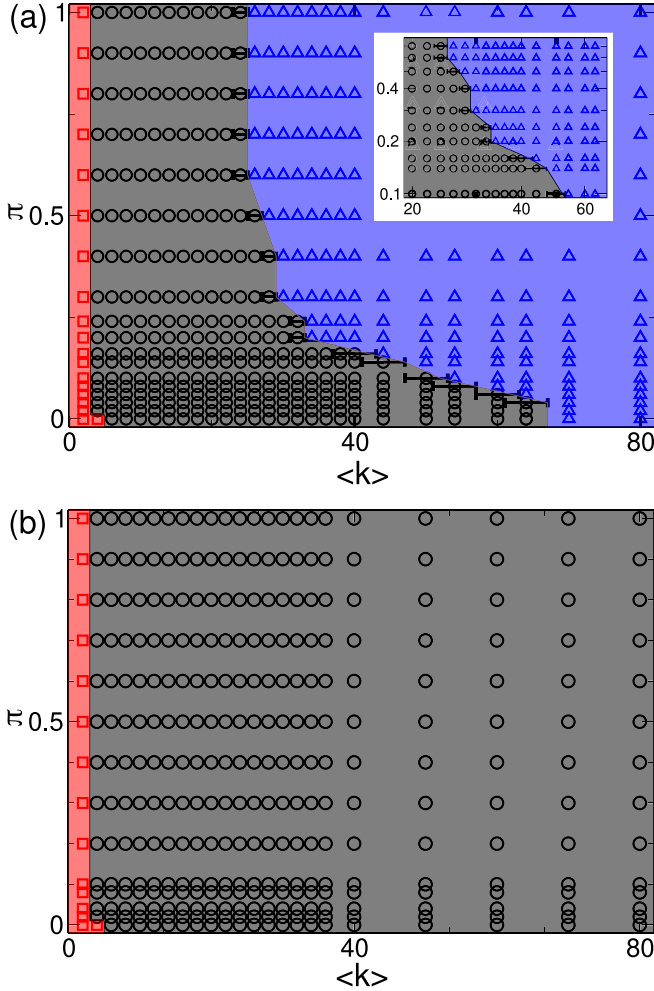


FIG. 5. Classes of collective dynamics emerging at different network topologies for both models [GH model in panel (a), KC model in panel (b)]. The graphs summarize the dynamical regimes observed for a wide range of network parameters (average connectivity $\langle k \rangle$ and degree of disorder π). Blue regions (triangles denote the values tested) indicate those values for which the networks exhibited discontinuous phase transitions to collective oscillations. Black regions (with circles) indicate continuous phase transitions, and red regions (with squares) transient dynamics to inactivity without a phase transition. The inset in panel (a) depicts a portion of the same data plot in the main panel in log-log scale.

We have used the first autocorrelation coefficient $\rho(1)$ of the order parameter fluctuations and the presence or absence of hysteresis to identify whether a dynamic transition is present, and to distinguish continuous from discontinuous transitions. This observable is sensitive enough to system's state: it can be used to tune a system towards criticality [37]. None of the present results depend on the use of the autocorrelation to track the dynamics. The presence of phase transitions and hysteresis in these models has been studied with other observables, such as the fraction of active sites f_S , the variance of activity fluctuations $\sigma_{f_S}^2$, or cluster quantities such as the size of the largest or the second largest cluster (S_1 , or S_2) as in Refs. [11,12], yielding similar results. We used $\rho(1)$ because its computation is straightforward and easy to replicate, it is

almost parameter free, therefore very convenient for comparing two different models.

The key difference between the two models is in the rule that determines how the activity propagates from a given neuron to its connected neighbors. The GH model mimics a discrete integrate-and-fire process taking place in real neurons. There, the “decision” to fire is post-synaptic, based on the amount of total depolarization, on a small patch of membrane, produced by the contribution of hundreds of thousands of impinging neurons [notice the sum in Eq. (1a)]. Disregarding the spontaneous activation term, the rule in the GH model is completely deterministic. In fact it is equivalent to a discretized partial differential equation, where the state $S_I(t+1)$ of a post-synaptic neuron I at time $t+1$ depends only on local quantities: it is determined by the previous state of that neuron, $S_I(t)$, the contribution of all other presynaptic neurons J_1 to J_k at time t , the weights W_{ji} of the connections, and the excitation threshold, i.e., $S_I(t+1) = f[S_I(t), S_{J_1}(t), \dots, S_{J_k}(t), W_{I_{i=1..k}, J}, T]$.

In contrast, in the KC model the propagation rule is a probabilistic [notice the product Eq. (2a)] contagion-like process [31], where a single excited neuron determines, according to a prescribed value of σ_p , how many of all of the neurons that connects to will fire next time. Thus, here the decision of how many neurons will be activated is presynaptic: a spiking neuron J excites on average σ_p post-synaptic I neurons, independently of the state of the other neurons connected to the same I neuron. Since σ_p accounts already for the average out degree of the network, the rule in Eq. (2a) determines, for each J neuron independently, the probability that such active neuron will have no-descendants, one, or more than one descendant. It is then rather unsurprising that the KC model is insensitive to the network topology.

While GH model exhibits a wealth of possible behaviors as a function of network topology, such as synchronized activity close to the critical point, a critical region for a broad range of control parameters, or the existence of discontinuous transitions, the same is not observed in KC model. An important ingredient for having such behavior is the existence of a deterministic activation rule: In the Supplemental Material [34] we show results for a *probabilistic postsynaptic* model, inspired by the model in Ref. [39], that may be tuned from discontinuous to continuous transitions as the degree of randomness in the *transmitted activation* rule is increased. Also, to gain an insight on the source of the differences among this models, a simplified, mean-field version, of KC and GH models (where there is no refractory period, nor spontaneous activation) is analytically solved in the Supplemental Material [34]. It can be seen that the simplified *stochastic presynaptic* model has only one stable solution for each value of the control parameter σ , while the simplified *deterministic postsynaptic* model may have several solutions for the same value of T , as a function of the initial conditions.

Although this is not the focus of the present report, it is worth to mention that the KC model rule is biologically implausible. As explained above, the actual activation mechanism of a given neuron involves a myriad of influences (thousands in mammalian brains) over a very small area. In addition, one has to consider that the output of an active neuron, after propagating through its axon from

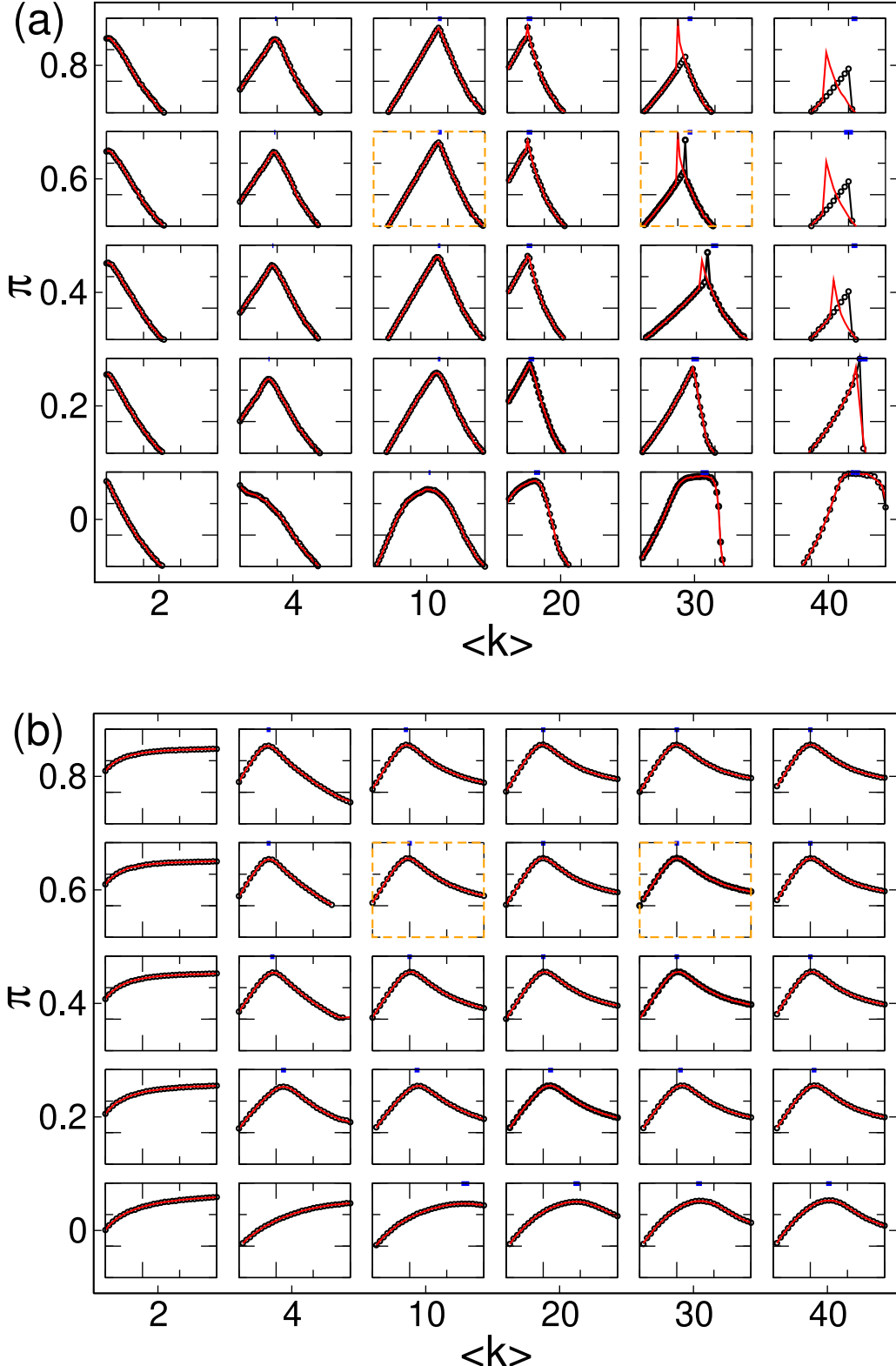


FIG. 6. Representative examples of the typical behavior of $\rho(1)$ as a function of the control parameter for diverse topologies in both models [GH model in panel a, KC model in panel (b)]. Simulations where run for 5×10^4 time steps for each value of T or σ_p , increasing (black circles) or decreasing (red lines) by $\Delta T = 0.005$ or $\Delta \sigma = 0.05$. For the GH model, x -axis range is $[0 : 0.3]$, for $\langle k \rangle = 2, 4$, and 10 , and $[0.2 : 0.5]$ for other $\langle k \rangle$ values. For the KC model, x -axis range is $\sigma_p = 0.5$ to $\sigma_p = 2$. y -axis range is $\rho(1) = 0.25$ to $\rho(1) = 1$ for both models. A thick blue dash over the upper x -axis marks a $\pm 3\%$ range of the control parameter, about its critical value (or T_+ for discontinuous transitions). The boxes remarked with dashed lines correspond to the parameters used in Figs. 2–4.

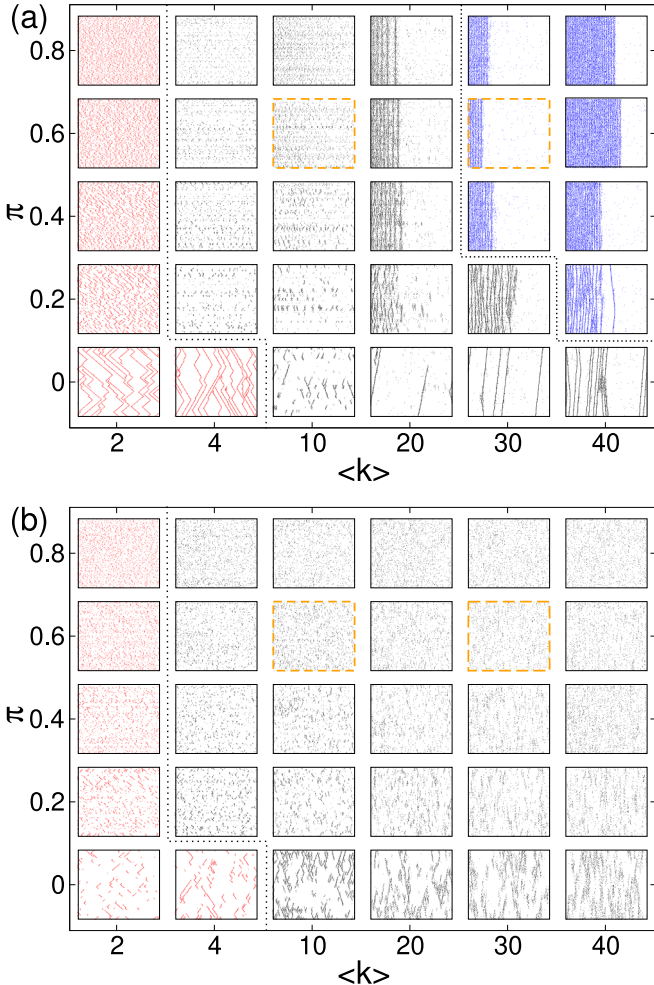


FIG. 7. Typical rasters of activity for networks with diverse topologies, while varying the control parameter around the critical value, for both models [GH model in panel a, KC model in panel (b)]. The dots in each box denote activity of a subset of 300 neurons (ordered in the y axis), for 300 time steps (x axis), as the control parameter is changed continuously about the critical point. Other network parameters as in Fig. 6. Dot color matches the regions of Fig. 5. The dotted black lines indicate the limits of the parameters that exhibit phase transitions. The boxes remarked with dashed lines correspond to the parameters used in Figs. 2–4.

hundreds of microns to millimeters, will stimulate all its contacts roughly *equally*. Thus, in order to excite a given number of neighbors, a given presynaptic neuron would actually have to have information on the number and state (active, refractory or silent) of the post-synaptic neurons and also of other presynaptic neurons attempting to excite the same neuron. This is biologically highly unrealistic, because the involved neurons may be centimeters away from each other, without a direct connection among them. Moreover, such hypothetically

very well informed J neuron will have to selectively cancel its stimulation strength with certain I neurons, as dictated by the value of σ_p , a requirement completely impossible for biological neurons.

Of course, the discussion above is not affecting the valuable points made in Ref. [15] where the KC model was introduced to show that a network of identical excitable elements achieves maximum dynamic range at criticality. Since the simulations in Ref. [15] were made on fixed topology networks (Erdős-Renyi) the present results are not affecting any of its conclusions which, is worth noticing, were replicated in many other models as well as in experiments. Less clear are the results in other cases, when the KC model was used to study the dynamics of non random topologies. These include the deviations from mean-field behavior found in scale free networks, as reported by Copelli and Campos [40] or Mosqueiro and Maia [41]. We note in passing that there are multiple instances in which the KC model was (mis)named as “Greenberg and Hastings stochastic model,” somewhat confusing according to the present results, as in the reports by Copelli and Campos [40], Wu *et al.*, [42], Asis and Copelli [43], Mosqueiro and Maia [41], to name only a few.

It is worth to note that the crucial influence of topology on the type of dynamics exhibited by excitable models has been discussed earlier by Kuperman and Abramson [44] in the context of epidemics. They found that the network degree and disorder determines the conditions at which endemic or epidemic situations occur.

To conclude, the point here is not that one needs super-realistic microscopic rules to build a valid model, but that microscopic rules do matter, and may lead to different collective behavior. In particular, we have shown that the KC model exhibits only one type of transition, independent of a large variation in the network topology. The observation that topology has an influence on the dynamics of certain models is fundamental at the present time, where several large-scale international scientific collaborations are devoted to map and study the consequences of features of the human brain connectome [45–47]. Examples include the numerical simulations using simplified models over derived connectomes, in order to understand brain functioning [10]. However, *not all neural models are the same*, and special care should be taken on the biases and limitations introduced by the applied models, before drawing conclusions on real brains.

ACKNOWLEDGMENTS

Work supported by the BRAIN initiative Grant No. 1U19NS107464-01. D.A.M. acknowledges financial support from ANPCyT Grant No. PICT-2016-3874 (AR) and the use of computational resources of the IFIMAR (UNMdP-CONICET) cluster.

[1] P. Bak, *How Nature Works: The Science of Self-organized Criticality* (Springer Science, New York, NY, 1996).
[2] D. R. Chialvo, *Physica A* **340**, 756 (2004).

[3] D. R. Chialvo, *Nat. Phys.* **6**, 744 (2010).
[4] T. Mora and W. Bialek, *J. Stat. Phys.* **144**, 268 (2011).
[5] J. M. Beggs and D. Plenz, *J. Neurosci.* **23**, 11167 (2003).

- [6] T. L. Ribeiro, S. Ribeiro, H. Belchior, F. Caixeta, and M. Copelli, *PLoS One* **9**, e94992 (2014).
- [7] P. Expert, R. Lambiotte, D. R. Chialvo, K. Christensen, H. J. Jensen, D. J. Sharp, and F. Turkheimer, *J. R. Soc. Interface* **8**, 472 (2011).
- [8] D. Fraiman and D. Chialvo, *Front. Physiol.* **3**, 307 (2012).
- [9] E. Tagliazucchi, P. Balenzuela, D. Fraiman, and D. Chialvo, *Front. Physiol.* **3**, 15 (2012).
- [10] G. Ódor, *Phys. Rev. E* **94**, 062411 (2016).
- [11] A. Haimovici, E. Tagliazucchi, P. Balenzuela, and D. R. Chialvo, *Phys. Rev. Lett.* **110**, 178101 (2013).
- [12] M. Zarepour, J. I. Perotti, O. V. Billoni, D. R. Chialvo, and S. A. Cannas, *Phys. Rev. E* **100**, 052138 (2019).
- [13] R. P. Rocha, L. Koçillari, S. Suweis, M. Corbetta, and A. Maritan, *Sci. Rep.* **8**, 15682 (2018).
- [14] S. A. Moosavi, A. Montakhab, and A. Valizadeh, *Sci. Rep.* **7**, 7107 (2017).
- [15] O. Kinouchi and M. Copelli, *Nat. Phys.* **2**, 348 (2006).
- [16] V. Priesemann, M. Wibral, M. Valderrama, R. Pröpper, M. Le Van Quyen, T. Geisel, J. Triesc, D. Nikolić, and M. H. J. Munk, *Front. Syst. Neurosci.* **8**, 108 (2014).
- [17] W. L. Shew, H. Yang, T. Petermann, R. Roy, and D. Plenz, *J. Neurosci.* **29**, 15595 (2009).
- [18] C. Haldeman and J. M. Beggs, *Phys. Rev. Lett.* **94**, 058101 (2005).
- [19] N. Deschle, J. Ignacio Gossn, P. Tewarie, B. Schelter, and A. Daffertshofer, *Front. Comput. Neurosci.* **14**, 118 (2021).
- [20] D. R. Chialvo, *Chaos, Solitons Fractals* **5**, 461 (1995).
- [21] N. F. Rulkov, *Phys. Rev. E* **65**, 041922 (2002).
- [22] M. Girardi-Schappo, O. Kinouchi, and M. H. R. Tragtenberg, *Phys. Rev. E* **88**, 024701 (2013).
- [23] B. Ibarz, J. Casado, and M. Sanjuán, *Phys. Rep.* **501**, 1 (2011).
- [24] G. Ódor and J. Kelling, *Sci. Rep.* **9**, 19621 (2019).
- [25] A. Levina, U. Ernst, and J. Michael Herrmann, *Neurocomputing* **70**, 1877 (2007).
- [26] E. Izhikevich, *IEEE Trans. Neural Netw.* **14**, 1569 (2003).
- [27] S.-S. Poil, R. Hardstone, H. D. Mansvelder, and K. Linkenkaer-Hansen, *J. Neurosci.* **32**, 9817 (2012).
- [28] M. E. J. Newman and G. T. Barkema, *Monte Carlo Methods in Statistical Physics* (Clarendon Press, Oxford, 2001).
- [29] J. M. Greenberg and S. Hastings, *SIAM J. Appl. Math.* **34**, 515 (1978).
- [30] D. J. Watts and S. H. Strogatz, *Nature (London)* **393**, 440 (1998).
- [31] S. Zapperi, K. B. Lauritsen, and H. E. Stanley, *Phys. Rev. Lett.* **75**, 4071 (1995).
- [32] P. Alstrøm, *Phys. Rev. A* **38**, 4905 (1988).
- [33] D. J. Korchinski, J. G. Orlandi, S. W. Son, and J. Davidsen, *Phys. Rev. X* **11**, 021059 (2021).
- [34] See Supplemental Material at <http://link.aps.org/supplemental/10.1103/PhysRevE.104.064309> for complementary results and a description of the Fortran 90 and Python 3 codes uploaded to github (<https://github.com/DanielAlejandroMartin/Apparently-Similar-Neuronal>).
- [35] A. de Andrade Costa, M. Copelli, and O. Kinouchi, *J. Stat. Mech. Theory Exp.* (2015) P06004.
- [36] J. G. F. Campos, A. A. Costa, M. Copelli, and O. Kinouchi, *Phys. Rev. E* **95**, 042303 (2017).
- [37] D. R. Chialvo, S. A. Cannas, T. S. Grigera, D. A. Martin, and D. Plenz, *Sci. Rep.* **10**, 12145 (2020).
- [38] E. S. Loscar, E. E. Ferrero, T. S. Grigera, and S. A. Cannas, *J. Chem. Phys.* **131**, 024120 (2009).
- [39] R. Pazzini, O. Kinouchi, and A. A. Costa, *Phys. Rev. E* **104**, 014137 (2021).
- [40] M. Copelli and P. R. A. Campos, *Eur. Phys. J. B* **56**, 273 (2007).
- [41] T. S. Mosqueiro and L. P. Maia, *Phys. Rev. E* **88**, 012712 (2013).
- [42] A.-C. Wu, X.-J. Xu, and Y.-H. Wang, *Phys. Rev. E* **75**, 032901 (2007).
- [43] V. R. V. Assis and M. Copelli, *Phys. Rev. E* **77**, 011923 (2008).
- [44] M. Kuperman and G. Abramson, *Phys. Rev. Lett.* **86**, 2909 (2001).
- [45] H. Markram, *Nat. Rev. Neurosci.* **7**, 153 (2006).
- [46] A. P. Alivisatos, M. Chun, G. M. Church, R. J. Greenspan, M. L. Roukes, and R. Yuste, *Neuron* **74**, 970 (2012).
- [47] S. M. Sunkin, L. Ng, C. Lau, T. Dolbeare, T. L. Gilbert, C. L. Thompson, M. Hawrylycz, and C. Dang, *Nucleic Acids Res.* **41**, D996 (2012).